

THE ADVANCED RADIOMETRIC RAY TRACER: ARARAT FOR PLANT CANOPY REFLECTANCE SIMULATION

P. Lewis and J-P. Muller

Department of Photogrammetry and Surveying, University College London
Gower St., London WC1E 6BT, UK
e-mail:plewis@ps.ucl.ac.uk

Abstract

A Monte Carlo ray tracing system, known as 'the Advanced RADIometric RAY Tracer' (ARARAT) has been developed as a tool for simulating radiance as measured by remote sensing instruments. The system takes 3-D geometric models of vegetation and/or surface topographic data (Digital Elevation Model - DEM) with associated radiometric attributes, and renders a scene for given illumination conditions for a given set of sensor characteristics.

ARARAT has been designed primarily for use with plant geometric data generated with the UCL Botanical Plant Modelling System to provide a simulation system capable of realistically simulating directional radiance and reflectance to allow investigations of the dependence of the signal received at a remote sensing instrument on the complex radiometric and geometric properties of plant canopies.

The design philosophy and implementation of ARARAT are discussed in this paper, with reference to Monte Carlo methods of estimating the integral of the radiance rendering equation.

Results of simulated maize (*Zea mais*) canopy reflectance are presented for the simple rendering case of singly-scattered directional radiance, and compared with values measured in the field.

KEY WORDS: Bidirectional Reflectance Distribution Function, Canopy Simulation, Monte Carlo Ray Tracing

1. Introduction

A numerical model of plant canopy and soil reflectance has been developed using the techniques of Monte Carlo ray tracing (see e.g. [Cook et al., 84], [Cook, 86], [Glassner, 89], [Muller and Dalton, 88]) to provide a tool for the realistic simulation of radiance measured by remote sensing instruments. Complex models of plant structure are generated by the UCL Botanical Plant Modelling System [Lewis, 90a] to allow the influence of the complex geometric and radiometric properties of a plant canopy on the radiation regime to be investigated. Models of underlying soil topography can be extracted by automated stereomatching of photogrammetric data as described in [Wall et al. 91]. The limitations of current canopy reflectance models are discussed in [Lewis, 90a] and [Gautier et al. 90] with particular reference to the lack of ability of classical radiative transfer models to simulate the influence of the complex structure of a plant canopy on its reflectance.

Monte Carlo techniques have been used previously in models of canopy reflectance (e.g. those developed by [Ross and Marshak, 88]) to solve the complex numerical integrations involved, using a simple structure to represent plant scattering elements, and a mixture of perfect diffuse (Lambertian) and specular reflectance functions [Ross and Marshak, 89] to represent scattering by these elements. Such a model has proved useful in sensitivity studies investigating the influence of the generalized plant architectural parameters on the directional reflectance of simulated canopies. A wide range of Monte Carlo ray tracing techniques [Cook, 86] [Ward et al., 88] have been developed by the computer graphics community for image simulation.

An alternative method of simulating radiative transfer in

complex structural environments is a technique known as radiosity (originally developed by the thermal engineering community [Hottel and Sarofim, 67], and later picked up by the computer graphics community), in which a model of the transfer of energy flux between diffuse (Lambertian) surfaces is calculated through a form-factor matrix describing the proportion of each surface as viewed from every other surface in the scene [Goral et al., 84]. The radiosity equations are then solved to provide a view-independent simulation of the surrounding radiation regime. [Borel et al., 91] have used basic radiosity techniques to simulate directional reflectance from a simple model of plant architecture. [Goel, 91] has used radiosity methods to simulate the scattering of light in more complex models of canopy architecture produced by L-system grammars [Prusinkiewicz, 90].

Monte Carlo ray tracing has the disadvantage with respect to the radiosity method in that it produces view-dependent renderings, meaning that separate renderings are needed for a simulation of separate views of directional reflectance for a particular canopy with given illumination conditions, but it has a major advantage in that it is not limited to simple Lambertian models of reflectance, and that it does not need to make assumptions about the shape of the model primitives. Methods have recently been developed which combine radiosity and ray tracing techniques, such as that presented by [Sillion et al., 91] in which energy intensity distributions are stored throughout the model by a small number of spherical harmonics. Such methods have not yet been tested for applicability on model spaces containing hundreds of thousands of primitives, such as are currently used for vegetation canopy modelling with ARARAT, nor have some of the assumptions used in the technique been fully tested with regard to their radiometric accuracy for a complex scene.

2. A Monte Carlo Ray Tracing Simulation System for BRDF Simulation

2.1. A Detailed Physically-Based Rendering Model

The ray tracing system presented in this paper provides a detailed model of the physical processes of image formation in a remote sensing scenario. The histories of sampled electromagnetic waves are traced through their interactions with a complex 3-D representation of plant canopy structure and soil topography (represented as a Digital Elevation Model (DEM)) to output canopy radiance. The system can also be used at other scales, such as by representing smaller-scale terrain (typically sampled on a 25 m to 500 m grid) as a DEM with associated radiometric attributes.

Radiative flux transfer can generally be modelled in a ray tracer with as few assumptions as required by the scale, polarization attributes and wavelength range of the simulation. The current version of ARARAT assumes: (1) that the incident radiation is unpolarized and that all interactions with primitives in the model are non-polarizing; (2) that all radiation exitant from the scene is solar reflected (the nature of the solar irradiance model is discussed below); (3) that the atmosphere has no scattering or absorption effects on radiation in the scene (other than in producing a diffuse illumination model from scattered solar radiation (see below)).

No assumptions about the plant or canopy geometry are made for models generated with the plant modelling system, up to the scale of leaf reflectance and leaf-scale geometry, so that the system can be used in its primary task of providing a detailed understanding of the formation of canopy-scale directional reflectance.

2.2. Ray Tracing

Ray tracing as used in the computer graphics community [Glassner: 89] is a modelling system describing the interaction of electromagnetic radiation with surfaces and volumes with defined material radiometric properties which produces images of defined geometric models. The electromagnetic radiation is modelled as a wavefront which travels in a plane orthogonal to some path (the ray path) from a source of energy (e.g. solar illumination) to a sensing element (e.g. a remote sensing instrument on a satellite) via interactions with scattering elements. This (naive) ray tracing method is called forward ray tracing [Glassner: 89]. When considering the simulation of radiance in the direction of a particular sensor, it is much more computationally efficient to allow the ray to trace its history from the sensing element to the illumination source in the reverse direction, which is the method adopted in ARARAT (reverse ray tracing).

A single wave travelling along a path (a ray) is considered to have an associated spectral wavelength value and a value representing the attenuation of the radiance associated with the path of the wave as it travels through the model. The ray travels in a straight line between scattering elements and the attenuation is varied according to the reflectance and transmittance properties of the volumes and surfaces with which the ray intersects along its path. The integration of the radiance over the

field of view of the sensor is modelled as the sum of the sample wave radiance values (see 2.4).

2.3. Multispectral Ray Tracing - Ray Bundles

Provided all scattering (including refractive and diffractive) processes are modelled as a modulation of ray intensity, rays of different wavelengths can be grouped together to form a bundle of rays with associated spectrally-varying properties. This bundle of rays can then be considered to travel along the same path, with attenuations applied differentially to each of the individual rays according to the spectral radiometric properties of the scattering elements it meets. In this way, multispectral simulations at n wavelengths can be performed without the need to trace the history of the individual rays n times.

2.4. The Rendering Equation as a Function of Incident and Exitant Angles

For the imaging geometry defined in figure 1, the bidirectional reflectance distribution function (BRDF) defined by [Nicodemus et al., 77] for the reflectance hemisphere of some material is stated by [Slater, 80] as:

$$\text{brdf}(\theta_v, \phi_v, \theta_r, \phi_r) = \frac{dL_e(\theta_v, \phi_v, \theta_r, \phi_r; E_i)}{dE_i(\theta_v, \phi_v)} \quad (1)$$

where $dL_e(\theta_v, \phi_v, \theta_r, \phi_r; E_i)$ is the incremental radiance (in $\text{Wm}^{-2}\text{sr}^{-1}$) exitant from the material (the radiant flux per unit solid angle leaving the extended source area δA in the direction (θ_r, ϕ_r) per unit projected source area in that direction), and $dE_i(\theta_v, \phi_v)$ the incremental incident irradiance (incident radiant flux density) (Wm^{-2}). If the BRDF is a function of wavelength, it is called the spectral BRDF. The bidirectional transmittance distribution function (BTDF) is defined similarly for the transmittance hemisphere.

The directional reflectance properties of a surface are often cited as the bidirectional reflectance factor ($\rho(\theta_v, \phi_v, \theta_r, \phi_r)$, the BRF), a unitless quantity which relates the exitant radiance (L_e) to the equivalent exitant radiance from a flat Lambertian plane under the same illumination conditions (L_L), defined as [Milton, 87]:

$$\rho(\theta_v, \phi_v, \theta_r, \phi_r) = \frac{dL_e(\theta_v, \phi_v, \theta_r, \phi_r; E_i)}{dL_L(\theta_v, \phi_v, \theta_r, \phi_r; E_i)} \quad (2)$$

which gives:

$$\rho(\theta_v, \phi_v, \theta_r, \phi_r) = \pi \text{brdf}(\theta_v, \phi_v, \theta_r, \phi_r) \quad (3)$$

The bidirectional transmittance factor ($\tau(\theta_v, \phi_v, \theta_r, \phi_r)$, the BTF) is similarly related to the BTDF.

The spectral flux density $E_{\text{diffuse}}(\lambda)$ (in $\text{Wm}^{-2}\mu\text{m}^{-1}$) from a spherical radiance source $L_i(\lambda, \theta_v, \phi_v)$ (in $\text{Wm}^{-2}\text{sr}^{-1}\mu\text{m}^{-1}$) incident on the area δA is given by:

$$E_{\text{diffuse}}(\lambda) = \int_{\theta=0}^{\theta=\pi/2} \int_{\phi=0}^{\phi=2\pi} L_i(\lambda, \theta_v, \phi_v) \cos \theta_v \sin \theta_v d\phi_v d\theta_v \quad (4)$$

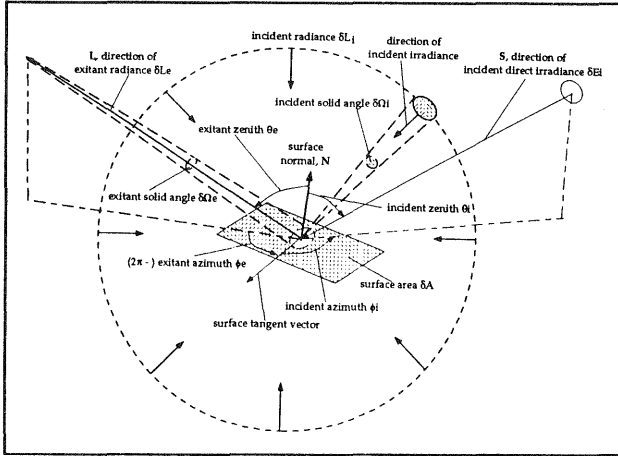


figure 1. Imaging Geometry - definition of angles

Since the diameter of the direct component of the solar irradiance presents an average angular subtense of about 0.5329° at the Earth's surface [Slater: 80], the Sun is usually considered to be a point source of irradiance. This will only be an invalid assumption if the BRDF of the surface is very sensitive to this magnitude of angular variation. The spectral flux density $E_{\text{direct}}(\lambda)$ (in $\text{Wm}^{-2}\mu\text{m}^{-1}$) due to a point light source $E_{\text{sun}}(\lambda)$ (in $\text{Wm}^{-2}\mu\text{m}^{-1}$) is given by:

$$E_{\text{direct}}(\lambda) = E_{\text{sun}}(\lambda) \cos(\theta_{\text{sun}}) \quad (5)$$

The total downwelling spectral flux density $E_{\text{total}}(\lambda)$ is then:

$$E_{\text{total}}(\lambda) = E_{\text{direct}}(\lambda) + E_{\text{diffuse}}(\lambda) \quad (6)$$

If an area δA is illuminated by a point spectral irradiance source $E_{\text{sun}}(\lambda)$ and a directional diffuse spectral radiance source $L_i(\lambda, \theta_i, \phi_i)$ surrounding the elemental area, the resulting spectral radiance $L_e(\lambda, \theta_r, \phi_r)$ is given from (1),(3),(4) and (5) by the rendering equation:

$$L_e(\lambda, \theta_r, \phi_r) = \int_{\phi_i=0}^{\phi_i=2\pi} \int_{\theta_i=0}^{\theta_i=\pi/2} L_i(\lambda, \theta_i, \phi_i) (\rho/\pi) \cos \theta_i \sin \theta_i d\phi_i d\theta_i + E_{\text{sun}}(\lambda) (\rho/\pi) \cos \theta_{\text{sun}} \quad (7)$$

where ρ is understood to represent the directional reflectance factor, BRDF ($\rho(\lambda, \theta_i, \phi_i, \theta_r, \phi_r)$) when the irradiance vector is on the same side of the patch δA as the exsitant radiance vector L_e , and the directional transmittance factor, BTF ($\tau(\lambda, \theta_i, \phi_i, \theta_r, \phi_r)$) otherwise. This can be expressed geometrically, given the incident irradiance direction vector S , the exsitant flux density direction L , and the local unit surface normal vector N as ρ represents BRDF if:

$$\text{sign}(S \cdot N) \neq \text{sign}(L \cdot N) \quad (8)$$

and $\text{sign}(x)=1$ if $x>1$ and $\text{sign}(x)=0$ if $x<1$. $\text{Sign}(x)$ is undefined for $x=0$. In equation (7), θ_i is assumed positive for the side of the patch for which θ_r is positive. A discussion of the general case of the rendering equation

formulated as an energy transfer between two points in a scene, reflected via a third is presented in [Kajiya, 86].

For a flat Lambertian plane, illuminated by a spatially variable incident sky radiance $L_{\text{sky}}(\lambda, \theta_i, \phi_i, \theta_{\text{sun}}, \phi_{\text{sun}})$ and direct irradiance E_{sky}, L_e in equation (7) reduces to $E_{\text{total}}(\lambda)/\pi$ and is constant for all viewing angles. Assuming constant sky radiance $L_{\text{sky}}(\lambda)$, the solution is simply:

$$L_e(\lambda) = L_{\text{sky}}(\lambda) + E_{\text{sun}}(\lambda) (1/\pi) \cos \theta_{\text{sun}} \quad (8)$$

In general however, equation (7) is not solvable by direct methods, especially for a complex canopy geometry, except by making simplifying assumptions about the canopy structure and the nature of the flux transfer.

The spectral albedo $\alpha(\lambda)$ is the hemispherical integral of spectral BRDF, and is a measure of spectral energy transfer between the sun and a material surface. The albedo α (the spectral albedo integrated over all wavelengths) is an important parameter in energy budget studies (e.g. [Dickinson et al., 90], [Kimes et al., 87]) and is defined as:

$$\alpha = \frac{\int_{\lambda} \int_{\phi_i=0}^{\phi_i=2\pi} \int_{\theta_i=0}^{\theta_i=\pi/2} L_e(\lambda, \theta_r, \phi_r) \sin \theta_r \cos \theta_r d\phi_r d\theta_r d\lambda}{\int_{\lambda} E_{\text{total}}(\lambda) d\lambda} \quad (9)$$

Note that as defined in equation (9), the albedo is implicitly a function of sun position (through the definition of L_e in (5) and through the dependence of the sky radiance on sun position), so a more useful measure of albedo might be obtained by integrating (9) over some (finite) time period.

2.5. Monte Carlo Sampling of the Rendering Equation

[Halton, 70] defines the Monte Carlo method as 'representing the solution of a problem as a parameter of a hypothetical population, and using a random sequence of numbers to construct a sample of the population, from which statistical estimates of the parameter can be obtained'. Monte Carlo techniques can thus be used to provide an estimate of the rendering equation (equation (7)), by transforming the integral to a summation equation, and randomly sampling the population of the summation. The problem is expressed as:

$$E[\tau] = \int \tau(\zeta) d\mu(\zeta) = \theta \quad (10)$$

where τ is known as the primary estimator of θ , and $E[\tau]$ is the expected value of the integral. Using the Monte Carlo method to evaluate (7), it is important to select a primary estimator for L_e so as to make $\text{var}[\tau]$ as small as possible. For m samples of τ :

$$\text{var}[L_{e,m}] = (1/m) \text{var}[\tau] \quad (11)$$

By setting $d\mu_i = 2\sin\theta_i \cos\theta_i d\theta_i$ in equation (7), so that $\mu_i = \sin^2\theta_i$, [Ward et al. 88] calculate a uniform segmented Monte Carlo distribution for the Lambertian reflection

case (ignoring the direct irradiance component for the present):

$$L_e(\lambda, \theta_r, \phi_r) = (1/2n^2) \sum_{j=1}^n \sum_{k=1}^{2n} L_i(\lambda, \theta_j, \phi_k) \quad (12)$$

$$\theta_j = \sin^{-1}(\sqrt{(j - X_j)/n}) \quad (13a)$$

$$\phi_k = 2\pi(k - Y_k)/n \quad (13b)$$

where X_j, Y_k are uniform random numbers between 0 and 1, for a total of $2n^2$ samples. This gives:

$$\text{var}[L_{e,2n \times n}] = (1/2n^2)\text{var}[L_i] \quad (14)$$

Considering the case for m random samples of diffuse reflectance over the Lambertian reflectance hemisphere gives:

$$L_e(\lambda, \theta_r, \phi_r) = (1/m) \sum_{j=1}^m L_i(\lambda, \theta_j, \phi_j) \quad (15)$$

with:

$$\theta_j = \sin^{-1}(\sqrt{X_j}) \quad (16a)$$

$$\phi_j = 2\pi Y_j \quad (16b)$$

and X_j, Y_j are uniform random numbers as before. The parameter m is the tree branching ratio. If m is set to 1, path tracing is performed, which [Kajiya, 86] claims to be a useful technique in variance reduction. This is because primary rays (first generation rays) (along with light source rays (shadow rays)) are the most important in terms of variance that they contribute to the pixel integral. Using a branching ratio of 1 thus ensures the maximum number of primary rays, making the random Monte Carlo sampling expressed in (15) preferable to the uniform stratified sampling of (13). Equations (15), (16) are implemented in ARARAT for diffuse irradiance sampling. To avoid excessive sampling of small contributions to the radiance from very deep nodes on the ray tree, the tree can be truncated at any desired depth. [Kirk and Arvo, 91] however warn against overuse of such a sampling strategy as it is likely to introduce a bias into the radiance estimate by eliminating a large number of small contributions.

Including anisotropic reflectance into equation (15) can be achieved by using:

$$L_e(\lambda, \theta_r, \phi_r) = (1/m) \sum_{j=1}^m L_i(\lambda, \theta_j, \phi_j) \rho(\lambda, \theta_j, \phi_k, \theta_r, \phi_r) \quad (17)$$

which is the sampling scheme currently implemented in ARARAT. However, equation (17) gives the variance of L_e as:

$$\text{var}[L_{e,m}] = (1/m)\text{var}[L_i(\lambda, \theta_j, \phi_j) \rho(\lambda, \theta_j, \phi_k, \theta_r, \phi_r)] \quad (18)$$

which will, in general be greater than that expressed in (14). This can potentially be overcome by incorporating ρ into the sampling scheme so that L_e is defined as in (15) and the variables $d\Theta$ and $d\Phi$ (both defined in the range [0,1]) are sampled with a uniform distribution. The relationship between $d\Theta, d\Phi$ and $d\theta, d\phi$ is then

$$d\theta d\phi = \rho(\lambda, \theta_j, \phi_k, \theta_r, \phi_r) \cos\theta_j \sin\theta_j d\theta_j d\phi_j \quad (19)$$

If (because of the complexity of ρ) it is not possible to obtain an analytical relationship between Θ, Φ and θ, ϕ from (19), a look up table (LUT) of the relationship could be set up for a uniform stratified distribution of $d\Theta d\Phi$ for sampled values of $\lambda, \theta_r, \phi_r$. However, this LUT could potentially be very large (e.g. for 128 samples in $\delta\Theta, 256$ in $\delta\Phi, 128$ samples in $\delta\theta_r$ and 256 samples in $\delta\phi_r$, a table of 1.07×10^9 samples would be required for each wavelength sample, for each defined material). Thus, such a sampling strategy is only really feasible if (19) can be solved analytically. An added complication arises if the relative magnitude of ρ varies over θ_i, ϕ_i with λ (i.e. the 'shape' of ρ varies with wavelength); which is discussed below.

Known sources of irradiance which can be considered as point sources or which have a small solid angle, such as the direct solar irradiance are targeted separately from the diffuse irradiance source, as expressed in equation (7). Such targeting is known as importance sampling [Cook, 86], and such rays fired towards a point light source are known as 'shadow rays', as they model the effect of dark cast shadows. A directional illumination source of finite field of view (FOV) can be modelled by distributing the direction of the shadow rays over the extent of the source FOV, producing penumbral effects [Cook et al., 84]. Stochastic sampling of the direct illumination source vector is implemented in ARARAT, in which the direct illumination vector is jittered over a disc around the principal solar direction.

3. The Fundamental Structure of The Ray Tracing Model - ARARAT

3.1. Design Philosophy

A ray tracing model, known as the Advanced RADIometric RAY Tracer (ARARAT) has been developed to allow the modelling of radiance measured by remote sensing instruments using ray tracing techniques on a model set of 3-D botanical plant and soil models. Figure 2 places ARARAT into the context of the UCL Botanical Plant Modelling System [Lewis, 90a]. ARARAT renders a radiance image in (byte or floating point) HIPL format [Landy, 83] (and provides the integrated radiance value

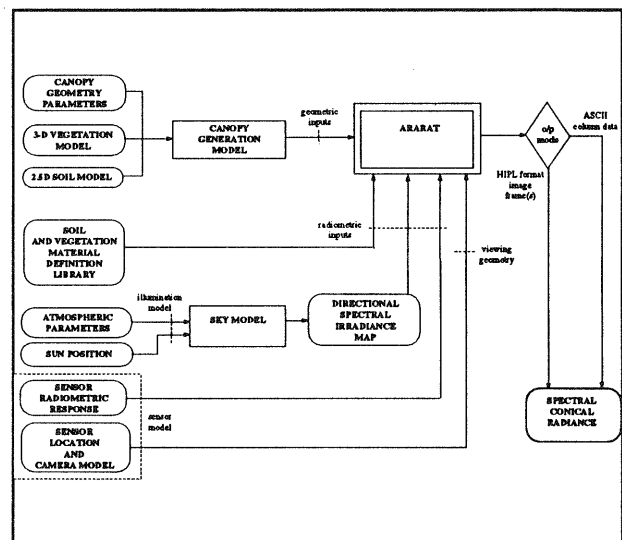


figure 2. ARARAT in the context of the UCL Botanical Plant Modelling System

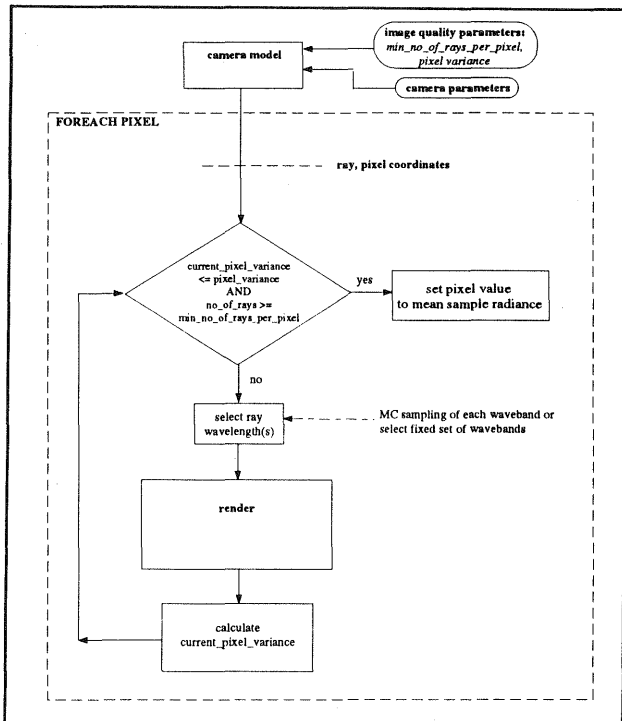


figure 3. functional diagram of ARARAT - origin and processing of primary rays

over the FOV of the sensor as ASCII data) for a given viewing geometry with given radiometric and geometric inputs. One important point to note about the system in its normal mode of use (with a very large number of scene primitives), is that the most computationally expensive part of the modelling is the intersection tests of sample rays with the elements of the geometric model. Efficient use of hierarchical bounding volumes around groups of plants and plant elements is used in designing the geometric model, but the intersection test is still by far the most costly part of the simulation.

The system is designed to be able to model both broad-band sensor spectral response functions (by Monte Carlo sampling of this function - see below) and spectroradiometric data with a large number of narrow wavebands. The ensuing requirement for a potentially large number of spectral samples coupled with the cost of scene intersection means that the spectral samples must be grouped into multispectral ray bundles for intersection, rather than being traced as individual single spectral value rays. Since the distribution described by the BRF is generally spectrally dependent, incorporating ρ into the Monte Carlo sampling scheme (via equation (19)) would result in the divergence of rays from the bundle. One possible solution to this would be to define a sampling scheme based on the mean value of $\rho(\lambda, \theta_i, \phi_i, \theta_r, \phi_r)$ over the wavelength range of interest, and to define the primary estimator τ relative to this mean reflectance function. However, since no satisfactory way is currently available for defining $\delta\theta, \delta\phi$, diffuse radiance is currently sampled relative to that of a Lambertian surface, and ρ is included in the primary estimator.

A major advantage of the Monte Carlo method is that increasing the dimensionality of the integral equation generally does not significantly increase the number of

samples required for convergence to a solution. Thus, integrating the radiance field both spatially and spectrally does not significantly increase the computation required for broad-band sensor response simulations. The number of samples required is mostly dependent on the requirements of the dimension of integration with the highest variability (i.e. spatial sampling in this case).

3.2. The Ray Tracing Model

Figure 3 shows a schematic of the fundamental processes of ray tracing implemented in ARARAT. Primary rays are 'fired' from the focal point of the camera model for each pixel on the camera imaging plane in a direction determined by the scanning characteristics of the camera model. The number of primary rays fired per pixel is determined by the lower bound threshold and the required variance of radiance of these ray samples. If N wavebands are to be modelled, the ray bundle contains N ray samples, where each ray sample has an associated wavelength value selected (for each primary ray sample) by Monte Carlo sampling of the sensor response function for that waveband. These rays are sent to the function 'render' which returns a set of ray radiance values.

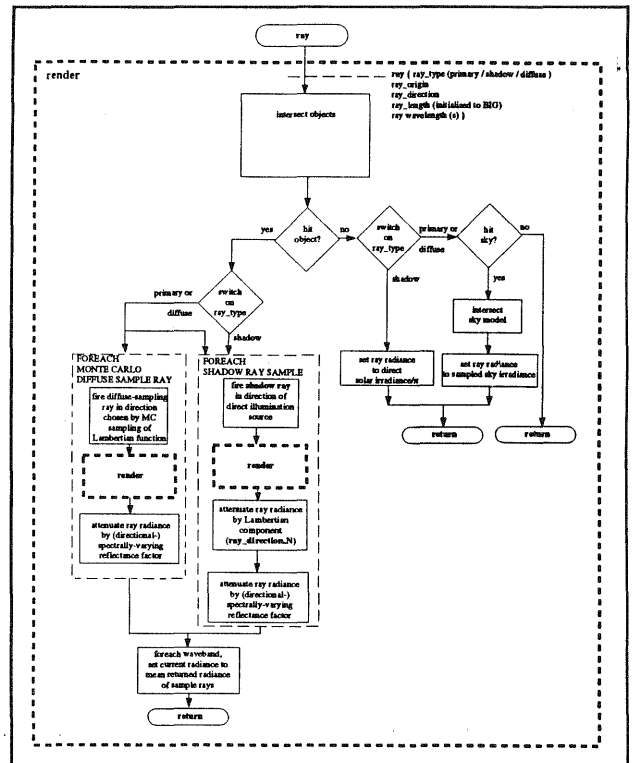


figure 4. functional diagram of the function 'render'

Figure 4 shows the processes involved within the function 'render'. A ray is tested for intersection with the geometric objects in the scene. If an object is intersected, and the ray is a primary or diffuse irradiance sampling ray, a set of m reflected and/or transmitted rays are propagated from the point of intersection in directions selected according to equation (15). This ray is then fed recursively into 'render' until a threshold ray depth is reached (noting the warning about ray tree truncation in section 2.5) or the ray does not intersect with an object. The returned ray radiance is then attenuated by ρ (since this is part of the primary estimator

function). A 'shadow ray' is also fired from the point of intersection with the model in order to sample the radiance due to the incident direct irradiance source. The shadow ray is passed into 'render' and the returned radiance sample attenuated by the product of ρ and the local Lambertian component (S.N from figure 1). Note that shadow rays do not propagate diffuse sampling rays.

If a ray does not intersect with a geometric object, it is given a sample radiance of E_{sun}/π if it is a shadow ray, and a radiance due to the local sky radiance in the direction of the ray sample otherwise.

3.3. The Primitive Set

The geometric primitive set currently incorporated into ARARAT consists of the following forms:

- (i) infinite plane
- (ii) sphere
- (iii) cylinder
- (iv) triangular facet
- (v) DEM object

Each object and grouping of objects is defined in an ASCII file in extended Wavefront format [Lewis, 90a], which is the format output from the program 'interpret' in the UCL Botanical Plant Modelling System. Objects are grouped locally and hierarchically into bounding box structures, which are defined as containers in the extended format. Full definitions of intersection algorithms are presented in [Lewis, 92], but [Glassner, 89] describes various general algorithms. One point to note about the intersection algorithms implemented in ARARAT is that they allow the definition of a 2-D space (bounded by [0,1] in the (local) coordinate system) over the surface of the 3-D objects, which can be used for mapping materials locally to the objects. [Lewis, 92] describes, for example, the use of this mapping in defining high frequency surface features such as a leaf vein network as a bump map [Cabral et al., 87] onto the (low frequency) definition of a leaf surface.

3.4. Reflectance Functions

Reflectance functions and other materials are defined in a material library. There are two types of reflectance functions implemented in ARARAT: a Lambertian and an anisotropic model. The term 'reflectance function' is intended to apply to the definition of a transmittance function as well.

The anisotropic model currently implemented is that of [Pinty et al., 90], [Verstraete et al., 90], which parameterizes a vegetation canopy as function of leaf area density, leaf angle distribution, average single scattering albedo, the radius of the sun flecks on the leaves, an asymmetry factor (defining the preferential scattering direction via the (empirical) Henyey-Greenstein phase function, and the incident and exitant radiation directions. The model is typical of such 'radiative transfer' models in that the leaves (scattering elements) are assumed to be randomly distributed throughout the canopy 'layer'. The model has been implemented based on code provided by the authors of the model, and has been incorporated into ARARAT

because it is able to model phenomena typical of vegetation canopies, such as the retroreflection peak (the hot spot). The model can also be used to model forward scattering peaks (specular reflection) by using a positive asymmetry factor in the phase function, but it is probably better to define a different physical directional reflectance function for non-plant canopy material surfaces (e.g. that described by [He et al., 91]), or to make use of general functional descriptions, such as spherical harmonics (e.g. [Sillion et al., 91]).

3.5. The Illumination Model

The illumination model in ARARAT is a set of sources of irradiance at an infinite distance from the geometric model. When a ray escapes from the bounds of the geometric model, it may then intersect any (relevant) illumination source. The (total or sampled) irradiance associated with this source is then propagated back along the path of the ray to the point of origin of the primary ray (the imaging plane), which is then given the appropriate radiance value. There are two types of illumination sources used in ARARAT - a direct source, representing the contribution of the direct (i.e. not scattered) solar irradiance, and a (hemispherical) distributed source, representing irradiance from the sky (i.e. solar irradiance which has been scattered by the atmosphere).

The direct source can be modelled as a point light source, or as a disc of defined arc, representing irradiance from the 'solar disc' (i.e. the extent of the sun as seen through the atmosphere).

Illumination data for input to the ray tracer can either be measured or modelled. [Ahmad et al., 87] describe the use of the NASA/GSFC PARABOLA spherical-scanning field radiometer [Deering and Leone, 84] in taking multidirectional irradiance measurements, from which the total diffuse sky irradiance is calculated and compared with a standard reference set of diffuse radiances. [Wilson, 91] describes the ATLAS instrument which is currently under development at BNSC-RSADU. It will be able to provide high spectral resolution measurements of direct- and diffuse-irradiance using two Spectron SE-590 heads mounted on an altazimuth platform controlled by a portable computer.

[Zibordi and Voss, 89] describe a simple model of directional spectral sky irradiance based on an approximate solution of the radiative transfer equation for a cloudless, homogeneous plane parallel atmosphere bounded by a Lambertian surface. The model is compared with measured data and found to agree in most cases to about $\pm 10\%$ for a range of solar zenith angles and wavelengths. The Zibordi-Voss model has been implemented in the Department of Photogrammetry and Surveying at UCL [Newton et al., 91], and can directly provide direct-solar and diffuse-sky spectral irradiance data in a format for input to ARARAT, given the appropriate parameters. Default parameters are provided for the sky model, but the following can be input if measurements or estimates are available:

- (i) the exoatmospheric solar radiance at the mean Sun-Earth distance

- (ii) atmospheric Ozone absorption spectra
- (iii) atmospheric Water vapour absorption spectra
- (iv) atmospheric absorption spectra of the 'uniformly mixed gases'

The model takes a coefficient of Ozone concentration and atmospheric precipitable Water vapour, as well as parameters of the Angstrom formula for total Aerosol optical thickness. It also requires coefficients of Ozone single scattering albedo, mean surface Lambertian reflectance, and parameters of the two term Henyey-Greenstein analytical function (to approximate the Aerosol phase function).

ARARAT requires the diffuse sky irradiance to be a HIPL format [Landy, 83] byte or floating-point multiple-frame image, where each frame represents spectral sky irradiance ($\text{mW cm}^{-2} \mu\text{m}^{-1} \text{sr}^{-1}$) for a particular wavelength as a function of zenith and azimuth angles. The direct irradiance data is read from a single column ASCII file.

3.6. The Camera Model

There are currently two camera models implemented in ARARAT: a central perspective camera (with a finite field of view (with sampling of the field of view as in [Glassner, 89], and the integrated radiance calculated as in [Rushmeier et al., 91]); and an 'albedo' camera model, which simulates the integrated hemispherical radiance by uniformly segmenting the exitant hemisphere according to (13) (the albedo integrated over each waveband is calculated by dividing this by E_{total} from (6)).

Because of the modular design of the ray tracer, it is relatively simple to incorporate new camera models to describe the origin and direction of primary rays for any particular scanning system, e.g. that of the MODIS remote sensing instrument [Salomonson, 89] which will appear on the EOS platform at the end of this century, so that data from such specific instruments can be realistically simulated.

A spectral response function can be defined for each waveband which allows Monte Carlo sampling of wavelength over the defined waveband [Newton, 91]. For a non-impulse response function, a wavelength is selected from the stratified Monte Carlo sampling limits for each waveband for each primary ray. The Monte Carlo simulation thus provides an estimate of the convolution of the response function with the radiance perceived by the sensor.

For a stratified Monte Carlo sampling scheme of the sensor relative spectral response (RSR) with n intervals, bounds λ_i , $i=1, \dots, n-1$ are defined so that:

$$\int_{\lambda_{i-1}}^{\lambda_i} \text{RSR}(\lambda) d\lambda = 1/n \int_{\lambda_0}^{\lambda_n} \text{RSR}(\lambda) d\lambda \quad (19)$$

where λ_0 and λ_n are the lower and upper wavelength bounds of the sensor response function respectively. For an impulse response function, the wavelength in a particular band is set the same for all primary rays.

4. Ray Tracing Techniques and Efficient Rendering Algorithms

4.1. Bounding Boxes

[Rubin and Whitted, 80] as cited in [Arvo and Kirk, 87] developed one of the first hierarchical bounding box algorithms in ray tracing to avoid an exhaustive search for ray intersections with all defined objects in a scene. This has become a widely-used technique, by which local groupings of primitives form bounded hierarchical collections (e.g. bounding boxes). Ray intersection tests are then performed on this hierarchy to localize the set of primitives requiring more complex testing algorithms. Bounding rectangular boxes are the only bounding volume primitives currently implemented in ARARAT, but [Glassner, 89] demonstrates that other regional bounds such as bounding spheres and cylinders should be used where appropriate. [Glassner, 89] provides an efficient bounding box intersection algorithm, which is implemented in ARARAT.

4.2. Local Plane-Sets

[Kay and Kajiya, 86] introduced the concept of plane-sets in a bounding volume for efficient ray tracing. In this method, the set of object primitives in a scene is tested for ray intersection in a predefined order, which is determined from the local extent of each primitive space when projected into each plane-set. This technique is used locally within each bounding box in ARARAT, with the positive and negative coordinate system basis vectors providing 6 sorting directions.

If a ray intersects a bounding volume, the ray direction vector is processed for classification as being most closely aligned to one of the 6 sorting directions. The contents of each bounding box are ordered in a linked list as part of the geometric model parsing operation for each of these directions. In this way, objects are checked for intersection in approximately the same order as they are encountered along the ray vector.

4.3. Clones

In order to reduce the number of primitives required to simulate a field of plants (typically 126000 primitives for 142 plants), virtual copies of groupings of objects (clones) can be defined. These clones can have 2 simple geometric transformations applied to them to allow greater variability in the plants within a field - they can be rotated about the (global) z-axis at the global origin, and they can be translated in 3-D space to allow clones of plants to be seeded about a field. Thus, a set of plant models are defined at the origin of the coordinate system, are rotated about the z-axis, and then translated to some location in a field.

For example, using 5 defined plant models with the plants as translated rotated cloned models would require of the order of only 4600 primitives to be stored.

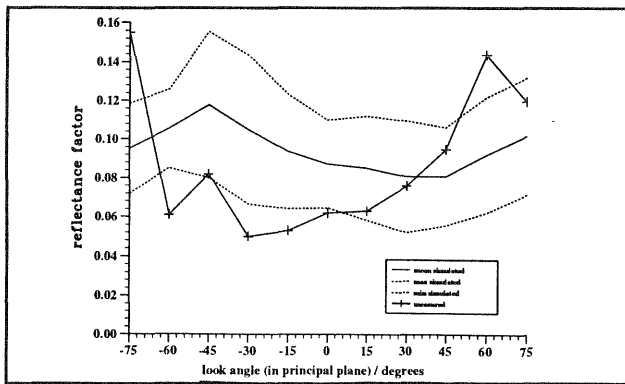


figure 5. simulated and measured directional reflectance in the solar principal plane for a planophile maize canopy

5. Results

5.1. Simulation of Maize Canopy Reflectance

An experiment was run to compare simulated reflectance of a maize canopy with directional measurements taken in the field by an SE-590 spectroradiometer [Milton, 87] with a 15° FOV, held on a boom at 1.4m from the top of the canopy. Field measurements were carried out at the Oxford University field station, in Wytham, Oxfordshire over the period of growth of the maize canopy. The results presented in this paper are those collected on July 4th 1990 between 0840 and 1010 GMT for a canopy sown at the beginning of May. The simulation was performed on plant models generated from key plant parameter measurements [Lewis, 90] by the UCL botanical plant modelling system. Canopy characteristics (row spacing, plant densi-

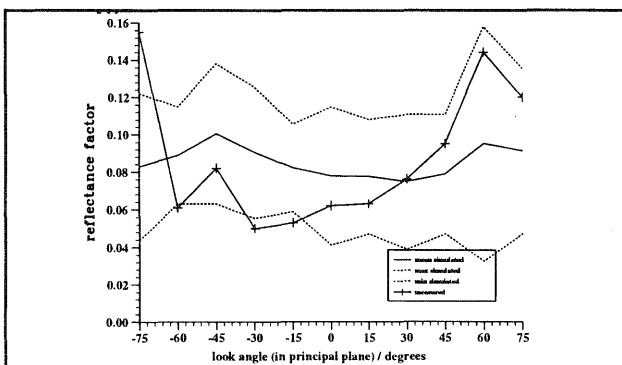


figure 6. simulated and measured directional reflectance in the solar principal plane for an erectophile maize canopy

ty etc.) were sampled directly in the field. The canopy had a row azimuth of 170°, and the solar angles assumed in the simulation were 112.6° azimuth and 45.77° zenith. The radiance model was generated from default atmospheric parameters, and the leaf reflectance/transmittance values taken from [Woolley, 70] and assumed Lambertian. Soil reflectance values were derived from measured nadir soil reflectance measurements. Since no measurements were taken of the maize leaf angles for this particular data set, estimated values were used [Lewis 91], and a sensitivity study was conducted with respect to maize leaf angle (a modulation of the estimated angles at the base and tip of each leaf) and mean plant density. Figure 5 shows the simulated reflectance for the estimated plant (a planophile canopy) at 550 nm, where the error bounds shown represent the envelope of 3σ relative to the mean canopy

reflectance calculated over 10 separate simulations. The simulations were carried out with 160000 primary rays per sensor position, with the assumption of direct illumination only and no multiple scattering (i.e. no diffuse sampling) and took approximately 1 cpu hour for each simulation on a SUN Sparc 2 workstation. Figure 6 shows the measured reflectance (also at 550 nm) compared with a simulated canopy with a 'leaf angle modulation' of 0.4 (i.e. the angles at the base and tip of each leaf were multiplied by 0.4 to obtain a more erectophile canopy).

It is difficult to interpret these results because of the large variances observed in the simulations. This is largely due to the proximity of the radiometer to the canopy compared with the scale of the vegetation observed (the radiometer viewed an area of only 369x369 mm at nadir!) causing the estimated error envelopes to be so large. In spite of this and the fact that no diffuse sampling was performed (therefore no multiple scattering (except of radiation transmitted through a leaf from the sun) and no sky irradiance), the modelling system has proved able to simulate the shape of the directional reflectance quite well (considering the quality of the model inputs and measured data), as well as the magnitude of reflectance. The results would tend to indicate that the canopy was more erectophile than originally estimated. Visual comparison of photography of the plants taken in the field at the same time as the radiometric measurements would tend to back this up. The variation of the canopy reflectance with plant spacing (and hence leaf area index (LAI)) was also studied, and the results of this are presented in [Lewis, 92]. The simulated canopy shown in figures 5 and 6 had an LAI of 0.917 ± 0.082 (directly calculated from the geometric model).

6. Conclusions

The theory behind and implementation of ARARAT have been presented in the context of Monte Carlo sampling of the radiance equation for remote sensing simulation. The UCL Botanical Plant Modelling System, of which ARARAT forms a part, has proved to be capable of simulating very complex canopy environments, even at close range with a very limited set of plant characterization measurements. The next stage in developing the system is to simulate radiance at IFOVs encountered with airborne and satellite remote sensing instruments, at a variety of scales, using the 3-D plant models, as well as mapping directional reflectance functions onto smaller-scale terrain elevation data.

Acknowledgments

The authors would like to thank the NERC who supported the data collection and development of the plant models under grant GR3/7020 (Angular variations of reflectance in multiple look-angle satellite and aircraft data) and the development of ARARAT under the TIGER 3.1 initiative. Thanks also go to Dr. Frank Thompson (Oxford University, Plant Sciences), and Dr. Mike Barnsley and Kevin Morris (UCL, Geography) as co-participants in the field work, as well as Andy Newton and Tim Day (UCL Photogrammetry and Surveying) for useful discussions about ray tracing. Finally, the support of the UCL Photogrammetry and Surveying Computer Systems Manager, James Pearson is gratefully acknowledged.

Bibliography

- Ahmad, S.P., E.M. Middleton, and D.W. Deering, 1987. Computation of Diffuse Sky Irradiance from Multidirectional Radiance Measurements. *Rem. Sens. Env.*, Vol. 21, pp 185-200.
- Arvo, J., and D. Kirk, 1987. Fast ray tracing by ray classification. *Computer Graphics*, Vol. 21(4), pp 55-64.
- Borel, C.C., S.A.W. Gerstl, and B.J. Powers, 1991. The radiosity method in optical remote sensing of structured 3-D surfaces. *Rem. Sens. Env.*, Vol. 36, pp 13-44.
- Cabral, B., N. Max, and R. Springmeyer, 1987. Bidirectional reflection functions from surface bump maps. *Computer Graphics*, Vol.21(4), pp 273-281.
- Cook, R.L., T. Porter, and L. Carpenter, 1984. Distributed ray tracing. *Computer Graphics*, Vol. 18(3), pp 139-147.
- Cook, R.L., 1986. Stochastic sampling in computer graphics. In: *ACM Trans. Graphics*, Vol. 5(1), pp 183-304.
- Deering, D.W., and P. Leone, 1984. A Sphere-Scanning Radiometer for Rapid Directional Measurements of Sky and Ground Radiance: the PARABOLA Field Instrument. NASA Technical Memorandum 86171, NASA GSFC, Greenbelt, MD-USA.
- Dickinson, R.E., B. Pinty, and M.M. Verstaete, 1990. Relating surface albedos in GCMs to remotely sensed data. *Agric. For. Meteorol.*, Vol. 52, pp 109-131.
- Gautier, R.P., F.J. Ahern, P.M. Teillet, and G. Fedosejevs, 1990. Report on the specialist meeting on the derivation of bidirectional reflectance distribution functions for various ground cover types. Specialist meeting report, Tempe, AZ-USA.
- Glassner, A.S., 1989. *An Introduction to Ray Tracing*. Academic Press.
- Goel, N.S., I.Rozehnal, and R.L. Thompson, 1991. A computer graphics based model for scattering from objects of arbitrary shapes in the optical region. *Rem. Sens. Env.*, Vol. 36, pp 73-104.
- Goral, C., K.E. Torrence, D. Greenburg, and B. Battaile, 1984. Modelling the interaction of light between diffuse surfaces. *Computer Graphics*, Vol. 18(3), pp 213-222.
- Halton, J.H., 1970. A Retrospective and Prospective survey of the Monte Carlo method. *Siam Revue*, 12(1), pp 1-63.
- He, X.D., K.E. Torrance, F.X. Sillion, and D.P. Greenburg, 1991. A comprehensive physical model for light reflection. *Computer Graphics*, Vol.25(4), pp 175-186.
- Hottel, H.C., and A.F. Sarofim, 1967. *Radiative transfer*. McGraw-Hill.
- Kajiya, J.T., 1986. The rendering equation. *Computer Graphics*, Vol. 20(4), pp 143-150.
- Kay, T.L., and J.T. Kajiya, 1986. Ray tracing complex scenes. In: *Computer Graphics*, Vol. 20(4), pp 269-278.
- Kimes, D.S., P.J. Sellers, and W.W. Newcomb, 1987. Hemispherical reflectance variations of vegetation canopies and their implications for global and regional energy budget studies. *J. Climate and Applied Meteorology*, Vol. 26, pp 959-972.
- Kirk, D., and J. Arvo, 1991. Unbiased sampling techniques for image synthesis, *Computer Graphics*, Vol. 25(4), pp 153-156.
- Landy, M., 1983. The HIPL picture/header format standard. Human Information Processing Laboratory, Psychology dept., New York University, NY-USA.
- Lewis, P., 1990a. Botanical plant modelling for remote sensing simulation studies. Mphil/Ph.D. transfer dissertation, Dept. Photogrammetry and Surveying, University College London, London-U.K.
- Lewis, P., and J-P. Muller, 1990b. Botanical plant modelling for remote sensing simulation studies. In: *Proc. IGARSS'90*, Washington DC-USA, Vol. 3, pp 1739-1742.
- Lewis, P., J-P. Muller, and K. Morris, 1991. Quality assessment of a botanical plant modelling system for remote sensing simulation studies. In: *Proc. IGARSS'91*, June, Espoo-Finland, Vol. 4, pp 1917-1920.
- Lewis, P. and J-P. Muller, 1992. Albedo and BRDF simulation using Monte Carlo ray tracing of geometric plant models. *Rem. Sens. Reviews*, submitted.
- Milton, E.J., 1987. Principles of field spectroscopy. *Int. J. Remote Sensing*, Vol. 8(12), pp 1807-1827.
- Muller, J-P., and M.N. Dalton, 1988. Application of ray tracing to satellite imagery understanding. In: *Proc. IGARSS'88*, Edinburgh-U.K.
- Newton, A.C., J-P. Muller, and J. Pearson, 1991. SPOT DEM shading for Landsat-TM topographic correction. In: *Proc. IGARSS'91*, Espoo-Finland.
- Nicodemus, F.E., J.C. Richmond, J.J. Hsia, W.H. Venable Jr., I.W. Ginsberg, and T. Limperis, 1977. Geometrical considerations for Reflectance Nomenclature. NBS Monograph 160, US. Dept. of Commerce, 1977.
- Pinty, B., M.M. Verstraete, and R.E. Dickinson, 1990. A physical model of the bidirectional reflectance of vegetation canopies. 2. inversion and validation, *J. Geophys. Research*, Vol. 95(D8) pp 11767-11775.
- Prusinkiewicz, P., and Lindenmayer, A., 1990. *The Algorithmic Beauty of Plants*. Springer-Verlag.
- Ross, J.K., and A.L. Marshak, 1988. Calculation of canopy bidirectional reflectance using the Monte Carlo method. *Rem. Sens. Env.*, Vol. 24, pp 213-225.
- Ross, J.K., and A.L. Marshak, 1989. Influence of leaf orientation and the specular component of leaf reflectance on the canopy bidirectional reflectance. *Rem. Sens. Env.* Vol. 24, pp 213-225.
- Rubin, S., and T. Whitted, 1980. A three-dimensional representation for fast rendering of complex scenes. In: *Computer Graphics*, Vol. 14(3), pp 110-116.
- Rushmeier, H.E., J.M. Parker, and K-M. Lee, 1991. Physically accurate synthetic images for computer vision system design. report GIT-GVU-91-25, Graphics, Visualisation and Usability Center, College of Computing, Georgia Inst. Tech., Atlanta, GA-USA.
- Salomonson, V.V., W.L. Barnes, P.W. Maymon, H.E. Montgomery, and H. Ostrow, 1989. MOSIS: Advanced facility instrument for studies of the Earth as a system. *IEEE Trans. Geosci. and Rem. Sens.*, GE-27, pp 136-144.
- Sillion, F.X., J.R. Arvo, S.H. Westin, and D.P. Greenburg, 1991. A global illumination solution for general reflectance distributions. *Computer Graphics*, Vol. 25(4), pp 187-196.
- Slater, P.N., 1980. *Remote Sensing - optics and optical systems*. Addison-Wesley.
- Verstraete, M.M., B. Pinty, B., and R.E. Dickinson, 1990. A physical model of the bidirectional reflectance of vegetation canopies. 1. theory, *J. Geophys. Research*, Vol. 95(D8), pp 11755-11765.
- Wall, S.D., T.G. Farr, J-P. Muller, P. Lewis, and F.W. Leberl, 1991. Measurement of surface microtopography. *Photogrammetric Engineering and Remote Sensing*, Vol. 57(8), pp 1075-1078.
- Ward, G.J., F.M. Rubenstein, and R.D. Clear, 1988. A ray tracing solution for diffuse interreflection. *Computer Graphics*, Vol.22(4), pp 273-281.
- Wilson, A.K., 1991. ATLAS: An Auto-Tracking Land and Atmosphere Sensor for Retrieval of Atmospheric Optical Parameters and Acquisition of Bidirectional Surface Reflectance. In: *Proc. 5th Int. Colloq. Spectral. Signatures of Objects in Remote Sensing*, pp 463-466..
- Woolley, J.T., 1970. Reflectance and transmittance of light by leaves. *Plant Physiol.*, Vol. 47, pp 656-662.
- Zibordi, G., and K.J. Voss, 1989. Geometrical and Spectral Distribution of Sky Radiance: Comparison between Simulations and Field Measurements. *Rem. Sens. Env.*, Vol. 27, pp 343-358.